Characterization and Electrical Transport Properties of Polyaniline and Multiwall Carbon Nanotube Composites

G. CHAKRABORTY,[1] S. GHATAK,[1] A. K. MEIKAP,[1] T. WOODS,[2] R. BABU,[2] W. J. BLAU[2]

[1]Department of Physics, National Institute of Technology, Durgapur Mahatma Gandhi Avenue, Durgapur 713 209, West Bengal, India

[2]Physics Department, University of Dublin, Trinity College, Dublin 2, Ireland

Received 15 July 2009; revised 19 March 2010; accepted 13 April 2010
DOI: 10.1002/polb.22042
Published online in Wiley InterScience (www.interscience.wiley.com).

ABSTRACT: Polyaniline/multiwalled carbon nanotube (PANI/MWNT) composites were prepared by *in situ* polymerization. Scanning electron microscope, X-ray diffraction, Fourier transform infrared, Uv-Visible spectroscopy, Fluorescence spectrophotometry were done to characterize the PANI/MWNT composites. Thermal stability was measured by thermogravimetry analysis. The thermal stability of PANI/MWNT composites becomes higher than PANI. Electrical transport properties of different PANI/MWNT composites were investigated in the temperature range $77 \leq T \leq 300$ K with and without magnetic field up to 1 T. The dc resistivity of PANI/MWNT composites shows different behavior compared to the sample without MWNT. The room temperature dc magnetoconductivity of the samples is negative; however, its sign changes to positive by lowering the temperature, which has been explained by hopping type charge transport. © 2010 Wiley Periodicals, Inc. J Polym Sci Part B: Polym Phys 48: 1767–1775, 2010

KEYWORDS: carbon nanotubes; charge transport; conducting polymers; conductivity; FTIR; magnetoconductivity; multiwalled carbon nanotubes; polyaniline

INTRODUCTION

Polymers that are capable of conducting electricity due to partial oxidation or reduction (i.e., doping), are prospective classes of materials. They possess an extended π-conjugation along the polymer backbone and exhibit semiconducting behavior. During the last few decades, electrical transport in such conducting polymers has been thoroughly studied.[1–8] After the report of preparation of carbon nanotubes and polymer composites by Ajayan et al.,[9] there have been efforts to combine carbon nanotubes and polymers to produce functional composite materials with desirable electrical and mechanical properties.[10–12] Hence some properties of polymer have been exploited by incorporating the nanomaterials into the polymer matrix. Carbon nanotubes have attracted considerable attention due to their potential applications in electronic devices[13,14] and nanocomposites.[15,16] They have unique structural, mechanical, electronic, and thermal properties[12,17] and are attractive building blocks for the development of novel polymer-nanocomposite materials with enhanced functionality, especially if it comes to enhanced conductivity, thermal stability, and reinforcement properties.[19–21] Polyaniline (PANI) is taken as matrix material for our work, because not only it is highly stable in air and in some solvents, but also exhibits dramatic changes in its electronic structure and physical properties. Polymerization in the presence of carbon nanotubes leads to a more planar conformation of PANI along multiwalled carbon nanotubes (MWNTs). This is stabilized by strong π–π interactions between both components and accompanied by simultaneous self alignment of MWNTs. Because of the formation of conducting polymer-CNT networks, these materials are of interest for electronic applications including photovoltaic cells, organic light emitting diodes, electromagnetic shielding, electro static dissipation, antennas, and batteries.[13,14,21–23] During the last decade, many investigations have been reported regarding the morphology and enhancement of conductivity by combining CNT and conducting polymers in the literature.[24–43] Among them some authors[24–28] has studied how the room temperature conductivity of the composites changes with MWNT contents. One dimensional variable range hopping transport in PANI nanotubes doped with MWNT-$(OSO_3H)_n$ was reported by Wei et al.[29] Sainz et al.[30] presented a quite flat temperature dependence of conductivity due to the conduction through a percolated three dimensional network of MWNTs. Zhang et al.[31,32] and Long et al.[33] have studied the overall temperature dependence conductivity of PANI/MWNT composites. They have also shown the positive magnetoconductivity of this system.

Apart from the above studies, charge transport in conducting polymers remains a topic of significant controversy because of strong influence of disorder on the transport properties of conducting polymers.[44,45] Recently, potential applications in nanotechnology have generated a widespread interest in the study of the electronic transport of polymer/CNT composites.

Correspondence to: A. K. Meikap (E-mail: meikapnitd@yahoo.com)
Journal of Polymer Science: Part B: Polymer Physics, Vol. 48, 1767–1775 (2010) © 2010 Wiley Periodicals, Inc.

However, most of the studies have concentrated on preparation and characterization of polymer/MWNT composites,[24–43] only a few have been done on transport properties of polymer/functionalized MWNT.[46,47] On the other hand, a wide range of functionalized multiwalled carbon nanotubes is now available, opening the possibility of new class of nanocomposites with polymer. This inspired us to investigate the composites of different MWNT with conducting polymers for their electrical properties.

This work describes the synthesis and characterization of protonic acid doped PANI with MWNT and functionalized MWNTs fabricated by *in situ* chemical oxidative polymerization method. To show the effects of MWNT on the conductivity and magnetoconductivity of PANI/MWNT composites, we present the detailed electrical transport properties, such as dc conductivity and magnetoconductivity of PANI, PANI-MWNT, PANI-MWNT-COOH, and PANI-MWNT-NH_2 in the temperature range 77–300 K.

SAMPLE PREPARATION AND EXPERIMENTAL TECHNIQUE

PANI/MWNT composites were synthesized by *in situ* chemical oxidative polymerization directed with cationic surfactant cetyltrimethylammonium bromide (CTAB). In a typical synthesis process, 1.136 g CTAB and 60 mg MWNT (Nanocyl 3100, 3101, and 3152) were added in 300 mL 1(M) HCl solutions and sonicated to obtain well-dispersed suspensions, then cooled down to 1–5 °C in the refrigerator.

A precooled solution of 1.2 g (1.2 mL) aniline monomer is added to 125 mL 1(M) HCl solution and 2.72 g ammonium persulfate (APS) were added slowly with this solution and stirred magnetically for 5 min at ice chamber. After that the above well-dispersed MWNT/CTAB suspension is mixed with this solution. The reaction mixture was stirred for 30 min at ice chamber and then left standing in the refrigerator at 1–5 °C for 24 h. After that, the resulting black precipitate was filtered and washed with distilled water and methanol several times to remove CTAB, Oligomer, APS, and excesses HCl from the sample, and finally dried at room temperature in a dynamic vacuum for 24 h. Other two samples were prepared by the same procedure using MWNT modified with carboxylic acid groups (COOH) and amino group (NH_2). Two reference samples were prepared, one PANI and another MWNT with CTAB. To prepare PANI sample, a precooled solution of 1.2 g (1.2 mL) aniline monomer is added to 125 mL 1(M) HCl solution and 2.72 g ammonium persulfate (APS) were added slowly with this solution and stirred magnetically for 5 min at ice chamber and then left standing in the refrigerator at 1–5 °C for 24 h. After that, the resulting black precipitate was filtered and washed with distilled water and methanol several times to remove Oligomer, APS, and excesses HCl from the sample, and finally dried at room temperature in a dynamic vacuum for 24 h. The amount of produced products is in the range 0.65 to 0.75 g for different samples.

Fourier transform infrared (FTIR) spectra were recorded on a NEXUS, Nicolet FTIR spectrometer in the range 450–4000 cm^{-1} with KBr pellets. Thermal degradation studies were performed under N_2 gas with a Perkin-Elmer Instruments, Pyris1 TGA at heating rate of 10 °C/min from room temperature to 900 °C. The Uv-Vis spectrum of the samples was taken by a double beam spectrophotometer (Hitachi U-3010) using dimethylsulphoxide (DMSO) as a solvent. Photoluminescence (PL) spectra were recorded using a Hitachi Fluorescence Spectrophotometer (F-2500). We had used DMSO as solvent in sample preparation for Photoluminescence. We had studied the PL effect of all samples in room temperature for a fixed concentration. The X-ray diffraction (XRD) pattern was recorded using XPert pro X-ray diffractometer (PANLYTICAL) with nickel filter Cuk$_\alpha$ radiation ($\lambda = 1.5414$ Å) in 2θ range from 20° to 70°. The electrical conductivity of the samples was measured by a standard four probe method after ensuring good contact with highly conducting graphite adhesive (Electrodag 5513, Acheson, Williston, VT) and fine copper wires as the connecting wires. The dc conductivity was measured with an $8^1/_2$ – digit Agilent 3458A multimeter. The temperature dependence of the conductivity was studied with a liquid nitrogen cryostat. For the control and measurement of the temperature, an ITC 502S Oxford temperature controller was used. To measure the dc response, pellets of 1 cm in diameter of the samples was made by pressing the powder under a hydraulic pressure of 500 MPa. The magnetoconductivity was measured in the same manner by the variation of the transverse magnetic field ($B < 1$ T) with an electromagnet.

RESULTS AND DISCUSSION

FTIR spectrum of PANI and PANI with different MWNT composites are presented in Figure 1. PANI has characteristic peaks at 1629, 1560, 1490, 1360, 1250, 1200, 1100, 840

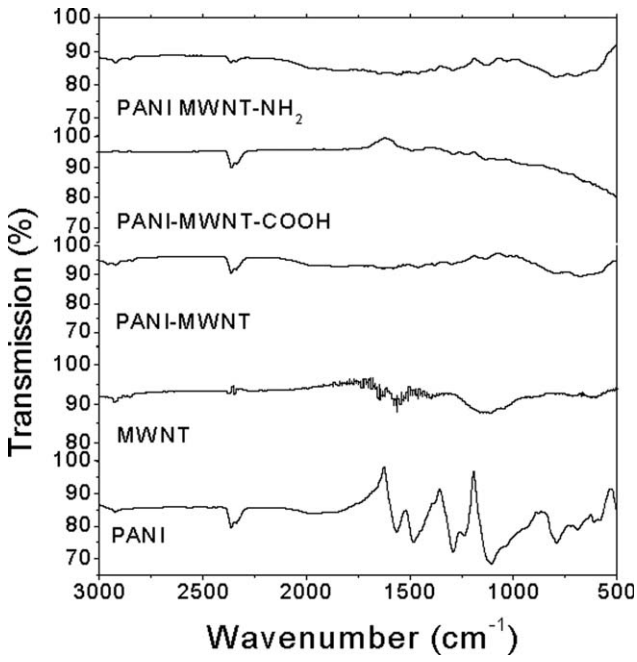

FIGURE 1 FTIR spectra of PANI, MWNT, and different PANI/MWNT composites.

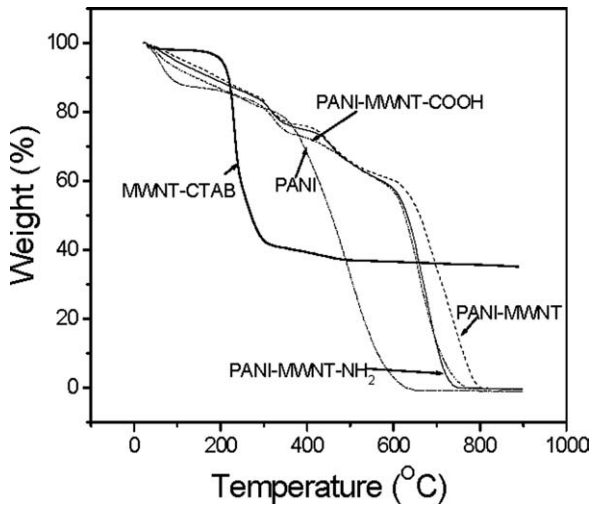

FIGURE 2 TGA curves of PANI, MWNT-CTAB, and different PANI/MWNT composites.

cm^{-1}. The band at 1627, 1560, and 1490 cm^{-1} attributed to C=C and C—C stretching modes of vibration for the quinoid (—N=Q=N, where Q = quinoid ring) and benzoid units.[48] The band at 1250 and 1200 cm^{-1} assigned to C—N stretching mode of benzoid unit of PANI. The band at 1100 cm^{-1} attributed to electronic band characteristic of conductivity of emeraldine salt PANI[49,50] and band at 840 cm^{-1} attributed to C—C and C—H stretching for the benzoid unit of PANI.[51] The peak assignment revealed that the produced product is PANI. FTIR spectrum of MWNT with CTAB is also shown in Figure 1. MWNT has characteristic peaks at 1570 and 1625 cm^{-1}. These peaks are assigned for C=C stretching vibration of MWNT. From the FTIR spectrum no characteristic changes are observed for CTAB. It was observed that incorporation of CNT in PANI provides a small shift (~3 to 5 cm^{-1}) in peak positions, decrease in peak intensity and structural change occurred. These changes occur due to the molecular interaction of PANI and CNT. The peak obtained at 1725 cm^{-1} for PANI-MWNT-COOH indicates the presence of C=O group of MWNT-COOH.[51]

Thermogravimetric analyses (TGAs) of different samples are given in Figure 2. The mass loss of the PANI samples began at around 50 °C and continued upto 110 °C. A rapid mass loss was also observed in between 400 to 600 °C. The initial mass loss was due to the loss of water molecules, and the next stage loss was due to the oxidative degradation of the polymer in air. MWNT-CTAB composite shows no mass loss upto 200 °C. From 200 to 300 °C about 60% mass loss occurs due to loss of CTAB molecule. About 40% masses retained upto 900 °C, because MWNT has not degraded in this temperature range. The PANI/MWNT composites did not show similar behavior. The samples started to degrade at higher temperature (600 to 750 °C) compared to PANI, which indicated a better stability for PANI/MWNT composites. As no mass loss is observed around 200 °C in our PANI/MWNT composites, we may conclude that CTAB is not present in the composites and CTAB has no effect on thermal stability of the investigated samples.

The photoluminescence (PL) spectra of PANI, PANI-MWNT, PANI-MWNT-COOH, and PANI-MWNT-NH_2 are shown in Figure 3. The excitation wavelength used was 300 nm. PL studies of different samples in solution were done at room temperature for a fixed concentration (10 mg per 2 mL DMSO). Hence DMSO was used as solvent in preparation of the solution. In presence of DMSO emeraldine salt is converted to emeraldine base. Therefore the PL intensity becomes low in PANI. The presence of MWNT influences the PL intensity of different samples. As seen from Figure 3, photoluminescence intensity of PANI-MWNT and PANI-MWNT-COOH samples is greater compared to PANI, however suppressed for PANI-MWNT-NH_2 sample. The maximum enhancement of intensity was observed in PANI-MWNT-COOH. This happens due to the combination of electron donating groups (>NH) in PANI and electron withdrawing group (>C=O) in MWNT-COOH, which enhances the π electron mobility in the composites. This in turn favors the formation of singlet excitons, which decayed radiatively to the ground state resulting in enhanced photoluminescence.[52] However, the presence of MWNT-NH_2 in PANI matrix may reduce the formation of singlet excitons, due to which the intensity may decrease in PANI-MWNT-NH_2 sample. The emission peaks is centered at around 449 nm for PANI, 434 nm for PANI-MWNT, 436 nm for PANI-MWNT-COOH, and 447 nm for PANI-MWNT-NH_2. This small decrease in peak position may be due to the presence of the defect state in between the energy gap of PANI.

In very dilute solution of PANI in DMSO emeraldine salt becomes deprotonated and gives the UV-Vis spectrum of emeraldine base.[53] In Figure 4a UV-Vis spectra of polyaniline and PANI-CNT composite shows two absorption bands at 330 and 630–660 nm, respectively. The first one is due to $\pi \rightarrow \pi^*$ transition in the benzoid ring and other is due to exciton absorption of the quinoid rings, respectively. In case of PANI-MWNT, MWNT interferes with the PANI backbone and $\pi \rightarrow \pi^*$ energy increases and therefore the wave length (λ) decreases. To obtain the absorption characteristics of the investigated samples, we have measured the transmittance

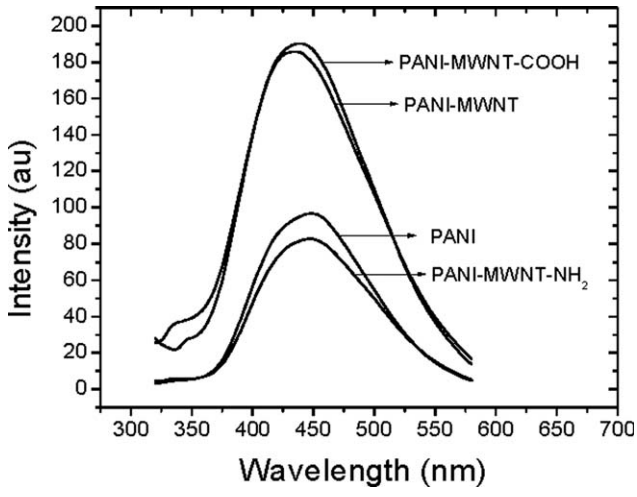

FIGURE 3 Photoluminescence spectra of PANI and different PANI/MWNT composites.

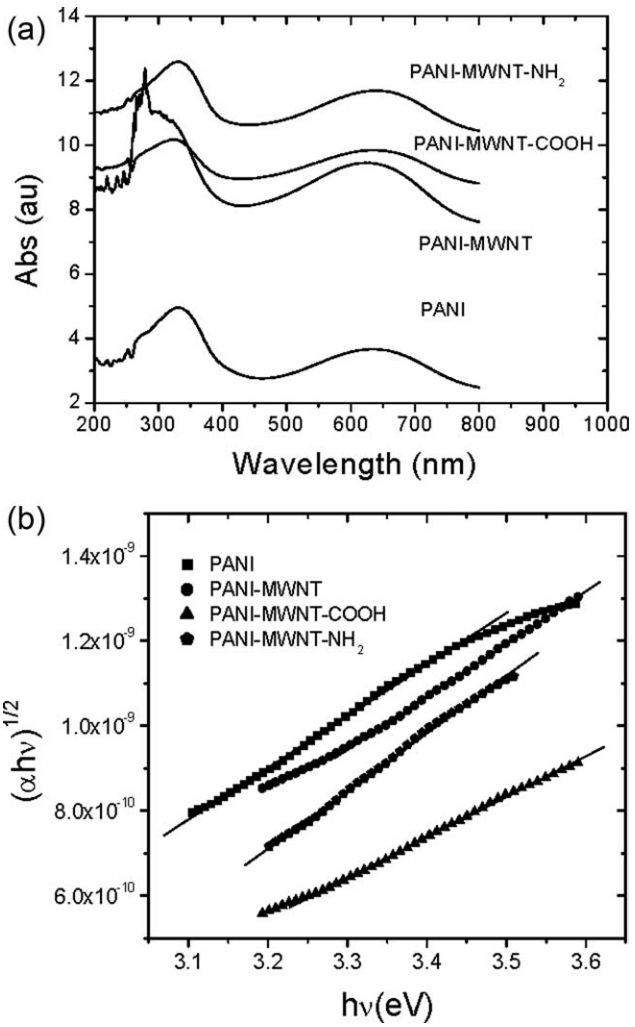

FIGURE 4 (a) UV-Vis spectroscopy of PANI and different PANI/MWNT composites, (b) Variation of $(\alpha h\nu)^{1/2}$ versus $h\nu$ of PANI and different PANI/MWNT composites.

(T) at different wavelengths (λ). The absorption coefficients (α) has been calculated by using the Beer-Lambert's relation

$$\alpha = \frac{1}{d}\ln\left(\frac{1}{T}\right) \tag{1}$$

where d is the path length. The absorption coefficient (α) is related with the incident photon energy ($h\nu$) by the following relation[54,55]

$$(\alpha h\nu)^{\frac{1}{m}} = C(h\nu - E_g) \tag{2}$$

where C is a constant and E_g is the optical bandgap of the materials and the exponent m depends on the type of the transition that is, $m = [1/2]$ for direct and allowed transition, 2 for indirect transition, and 3/2 for direct forbidden transition. To get the idea about optical band gap, a plot of $(\alpha h\nu)^{1/2}$ versus $h\nu$ has been done as shown in Figure 4(b). Then the band gap has been extracted by extrapolating the straight portion of the graph on $h\nu$ axis at $\alpha = 0$ and those are 2.46, 2.54, 2.63, and 2.68 eV for PANI, PANI-MWNT, PANI-MWNT-COOH, and PANI-MWNT-NH_2, respectively. It is observed that the bandgap increases by incorporating of different MWNT in PANI.

Figure 5 shows the XRD patterns of MWNT, MWNT+CTAB, PANI, PANI-MWNT, PANI-MWNT-COOH, and PANI-MWNT-NH_2. The difractogram of the pure MWNTs exhibits the typical peaks at 2θ angles 26°, 44°, and 51°, which corresponding to the graphite (002), (101), and (004) reflections, respectively.[19] In the difractogram of MWNT+CTAB sample some additional peaks are observed over MWNT peaks. It is also observed that peak intensity of MWNT is reduced without changing the peak position. This may be due to the presence of CTAB coating over MWNT. Therefore, it is clear that, from a structural point of view, no additional order has been introduced in MWNT in presence of CTAB. On the other hand, the PANI powders exhibit three broad peaks at 2θ angles 15°, 20.4°, and 25.2°, which are similar to those of the PANI reported by other groups.[24,56] These peaks in PANI may arise due to regular repetition of monomer unit aniline. When the different MWNT powders were incorporated into the PANI, the MWNT peaks corresponding to 44° and 51° are absent in the difractogram and the composites reveal their crystalline nature which is similar to pure PANI. This suggests that polymers are coated over the CNT. On the other hand, the peaks of the composites become much shaper and intensity is greater in compare to pure PANI due to the ordering of polymer chain along CNT. As no additional peaks due to CTAB have been observed in PANI/CNT composites, it may be confirmed that CTAB is not present in the composites and has no affect on the transport properties

The Figure 6 shows the scanning electron micrograph of pure MWNT [Fig. 6(a)], PANI-MWNT [Fig. 6(b)], PANI-MWNT-COOH [Fig. 6(c)], and PANI-MWNT-NH_2 [Fig. 6(d)] samples, respectively. A columnal growth has been observed

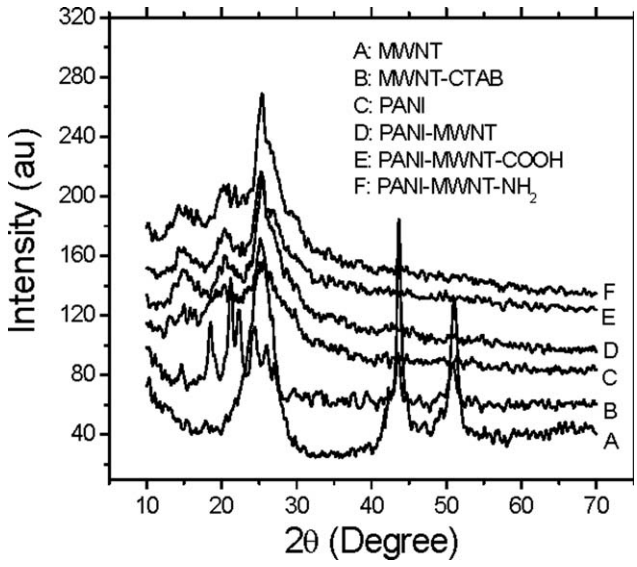

FIGURE 5 X-ray diffraction of MWNT, MWNT-CTAB, PANI, and different PANI/MWNT composites.

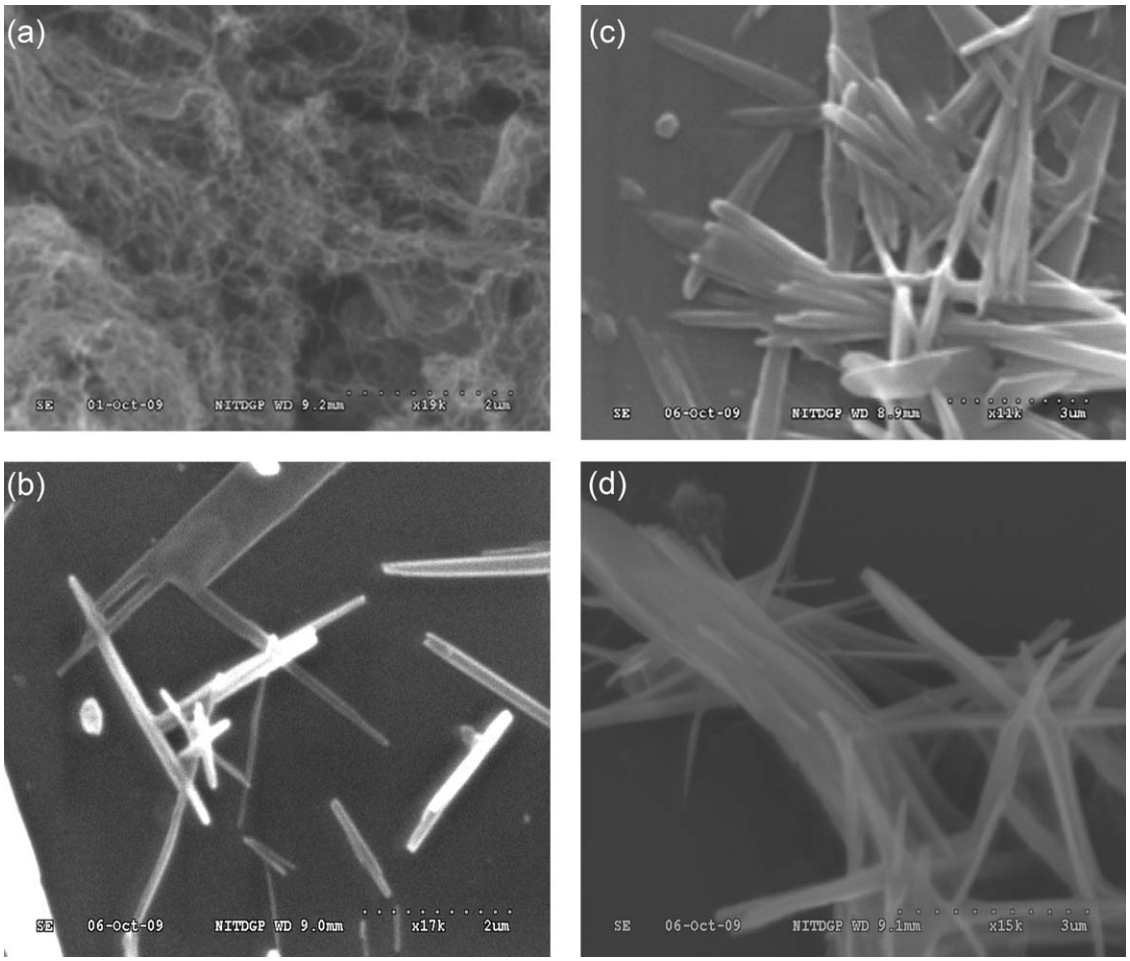

FIGURE 6 SEM image of (a) Pure MWNT (b) PANI-MWNT (c) PANI-MWNT-COOH, and (d) PANI-MWNT-NH_2.

in composites. Compare with the pure MWNTs, the diameter of the PANI/CNT composite becomes larger after *in situ* polymerization, which suggests that the aniline monomer is uniformly polymerized on the surface of the CNT and forms a columnal growth. Therefore, it is confirmed from SEM images that in all PANI/MWNT composites, polymers are coated over the CNT.

To explore how the CNTs affect the composite's resistivity, the dc resistivity of PANI/MWNT samples has been measured in the temperature range of $77 \leq T \leq 300$ K. The room temperature conductivity σ(300 K) and the conductivity ratio $\sigma_r = [\sigma(300\ \text{K})/\sigma(77\ \text{K})]$ increases by introducing the MWNT in polymer matrix from 0.44 to 1.79 $\Omega^{-1}\text{m}^{-1}$ and 1.39 to 3.93 respectively. Hence the increase in conductivity may be due to the presence of highly conducting carbon nanotubes. There is some interaction between the quinoid ring of the PANI and the CNT, which facilitate charge transfer processes between the two components. Because of a large π-conjugated structure in CNTs the localization length is around 10 nm, but for poorly conducting or amorphous PANI, it is around 2 nm.[57] Therefore the coupling between the CNT and polymer chains become stronger and enhances the average localization length, which results the increase in conductivity in PANI/CNT composites compared to PANI. The temperature dependence of resistivity for different investigated samples is shown in Figure 7. The resistivity increases with decrease of temperature, which is the characteristic behavior of semiconductor. Generally the temperature dependence of the resistivity $\rho(T)$ of disordered semiconducting materials is described by the Mott variable range hopping (VRH) model.[54] According to this model, the resistivity is given by

$$\rho(T) = \rho_0 \exp\left(\frac{T_{\text{Mott}}}{T}\right)^{\gamma} \tag{3}$$

where γ is the VRH exponent, which determines the dimensionality of the conducting medium. The possible values of γ are 1/4, 1/3, and $^1/_2$ for three, two, and one dimensional systems, respectively. ρ_o is the resistivity while $T \to \infty$, T_{Mott} is the Mott characteristic temperature, which usually depends on the electronic structure, and the energy distribution of the localized states, can be expressed as

$$T_{\text{Mott}} = \frac{16}{k_B N(E_F) L_{\text{loc}}^3} \tag{4}$$

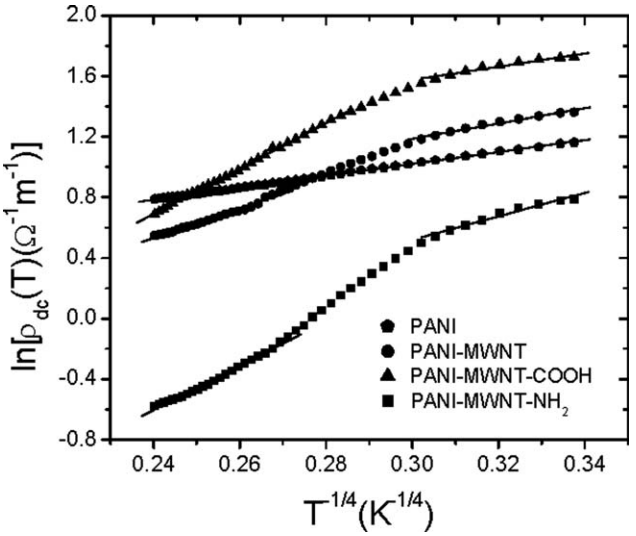

FIGURE 7 Temperature dependence of the dc conductivity of PANI and different PANI/MWNT composites. The solid lines are fitted to eq 3.

where k_B is the Boltzmann constant, $N(E_F)$ is the density of states at the Fermi level and L_{loc} is the localization length. To gain deeper insight into the mechanism of the electrical transport properties of the investigated samples, we have carefully analyzed the temperature dependences of resistivity in zero magnetic fields by using eq 3. Nonlinear behavior of the graph $\ln[\rho(T)]$ with $T^{-1/2}$ for all samples (not shown in manuscript) suggests that quasi one dimensional (1D) transport is not the dominating transport mechanism in PANI and PANI/MWNT composites. It is observed that PANI sample shows the linear variation in $\ln[\rho(T)]$ versus $T^{-1/4}$ plot for the full range of investigated temperature ($77 \leq T \leq 300$ K), which is shown in Figure 7. Therefore, the linear variation of $\ln[\rho(T)]$ with $T^{-1/4}$ indicates the prevalence of three dimensional (3D) charge transport ($\gamma = 1/4$) in the investigated sample. On the other hand, introduction of different MWNTs in PANI matrix show two different slopes in the plot of $\ln[\rho(T)]$ with $T^{-1/4}$ (Fig. 7). The values of T_{Mott} in two different temperature ranges (high temperature range $180 \leq T \leq 300$ K and low temperature range $77 \leq T \leq 130$ K) have been calculated from the slopes of the linear variation of $\ln[\rho(T)]$ with $T^{-1/4}$ and the estimated values of T_{Mott} are listed in Table 1. As shown in Table 1, the values of T_{Mott} at higher temperature increase by one to two orders of magnitude when compare with the T_{Mott} at lower temperature. The data demonstrate that the conductivity of the composites is dominated by CNT at lower temperatures. The value of $\gamma = 1/4$ indicates that our experimental result contradicts the quasi 1D transport in PANI and PANI/MWNT as observed by Long et al.[33] Wang et al.[58] reported that if the conducting chains are isolated, the quasi 1D VRH transport is important due to strong interchain coupling. However, this model breaks down if the conducting polymer chains are not isolated due to the presence of the conducting islands between the insulating matrix and the electronic wave function gets extended three dimensionally. It is observed from our SEM pictures (Fig. 6) that the conducting polymer chains are not isolated and the MWNT are embedded in PANI matrix. As a result the 3D VRH is responsible for the transport mechanism, which in our present investigation, derives confirmatory support by our experimental data.

TABLE 1 Conductivity Parameters like Conductivity at 300 K [σ(300K)], Conductivity Ratio [$\sigma_r = \sigma(300K)/\sigma(77K)$], and Mott Characterization Temperature (T_{Mott}) for Low and High Temperature Range

Sample	σ (300 K) ($\Omega^{-1}m^{-1}$)	σ_r	T_{Mott} (K) ($77 \leq T \leq$ 110 K)	T_{Mott} (K) ($180 \leq T \leq$ 300 K)
PANI	0.44	1.39	273	273
PANI-MWNT	0.58	2.26	330	10,341
PANI-MWNT-COOH	0.51	2.82	242	50,228
PANI-MWNT-NH_2	1.79	3.93	2,253	49,629

The magnetic field dependent conductivity of the samples has been measured under the influence of magnetic field of strength $<1T$. The variation of magnetoconductivity with magnetic field at $T = 300$ K for different samples is shown in Figure 8. It is observed that the room temperature magnetoconductivity of all samples is negative. The magnitude of the maximum percentage change of conductivity $[\{(\sigma(B, T) - \sigma(0, T))/\sigma(0, T)\} \times 100]$ in the presence of magnetic field of 0.8 T at 300 K was observed about 1.10% for PANI-MWNT-NH_2, which is greater than the value (0.3%) of PANI sample. So incorporation of MWNT-NH_2 in PANI matrix increases the magnetoconductivity more compared to the other samples like PANI with MWNT and MWNT-COOH. The measured magnetoconductivity data could be explained by simple phenomenological model that consists of two simultaneously acting hopping processes, namely the wave function shrinkage model[59,60] and the forward interference model.[61–63] The

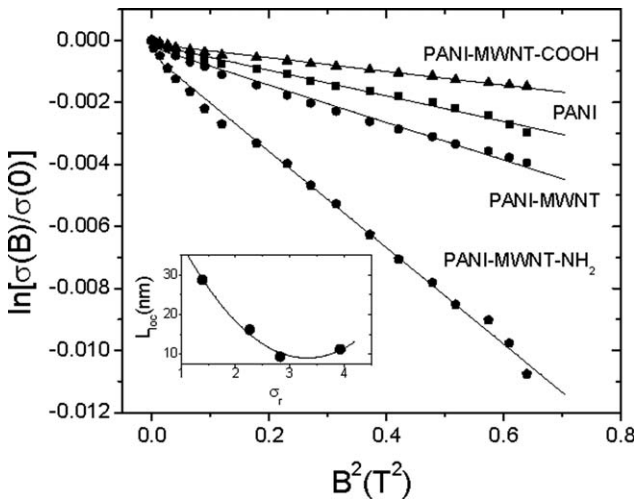

FIGURE 8 Variation of the dc magnetoconductivity with perpendicular magnetic field of PANI and different PANI/MWNT composites at 300 K. The solid lines are fitted to eq 5.

wave function shrinkage model corroborates the fact that by applying a magnetic field the wave functions of electrons are contracted and reduces the average hopping length. This corresponds to a negative magnetoconductivity (positive magnetoresitivity) that is, conductivity decreases with increasing magnetic field. For a small magnetic field, the magnetoconductivity ratio can be expressed by the following relationship[59]

$$\ln\left(\frac{\sigma(B,T)}{\sigma(0,T)}\right) = -t_1 \frac{e^2 L_{loc}^4}{\hbar^2}\left(\frac{T_{Mott}}{T}\right)^{3/4} B^2 \qquad (5)$$

where, $t_1 = 5/2016$ and L_{loc} is the localization length. On the other hand, the forward interference model takes into account the effect of forward interference among random paths in the hopping process between two sites spaced at a distance equal to the optimum hopping distance and the theory predicts the positive magnetoconductivity (negative magnetoresistivity), which can be expressed as:

$$\frac{\sigma(B,T)}{\sigma(0,T)} = 1 + \frac{\frac{C_{sat}B}{B_{sat}}}{1+\frac{B}{B_{sat}}} \qquad (6)$$

where C_{sat} is a temperature independent parameter and $B_{sat} = 0.7(h/e)(8/3)^{3/2}(1/L_{loc}{}^2)(T/T_{Mott})^{3/8}$. Because of a small localization length of PANI, the average hopping length $R_{hop} = (3/8)(T_{Mott}/T)^{1/4}L_{loc}$ is small and the wave function shrinkage effect is observed in PANI,[5] but this effect is not evident in CNT because of large localization length. A large negative magnetoresistance was widely reported for CNT at weak magnetic field and was interpreted in terms of the quantum interference effect.[64,65] Therefore, the sign and magnitude of the magnetoconductivity changes due to competition of the two (wave function shrinkage and quantum interference) types of contributions in PANI/MWNT composites. As the magnetoconductivity ratio of the investigated samples decreases with increasing magnetic field at a temperature 300 K, we assume that the contribution due to wave function shrinkage model predominated over the quantum interference model. So, we analyzed our measured data in the light of the wave function shrinkage model. Figure 8 shows a linear variation in the plot of $\ln[\sigma(B, T)/\sigma(0, T)]$ versus B^2 for different samples. The points are the experimental data while the solid lines represent the best fits obtained on the basis of the wave function shrinkage model. It is evident from the Figure 8 that the experimental data can be well described by the theory as indicated in eq 5. The localization length (L_{loc}) has been calculated from the slope of these lines in Figure 8 by using eq 5. The variation of the localization length with the conductivity ratio σ_r are shown in inset of Figure 8. The localization length decreases with increasing conductivity ratio. In the samples with higher disorder (σ_r large), the electronic wave functions are localized within smaller regions, resulting smaller localization length due to which the localization length decreases with increasing σ_r. Therefore, it may be concluded that the values of L_{loc} are strongly influenced by the presence of disorder of the samples because the extent of disorder is generally characterized in terms of the conductivity ratio (σ_r).

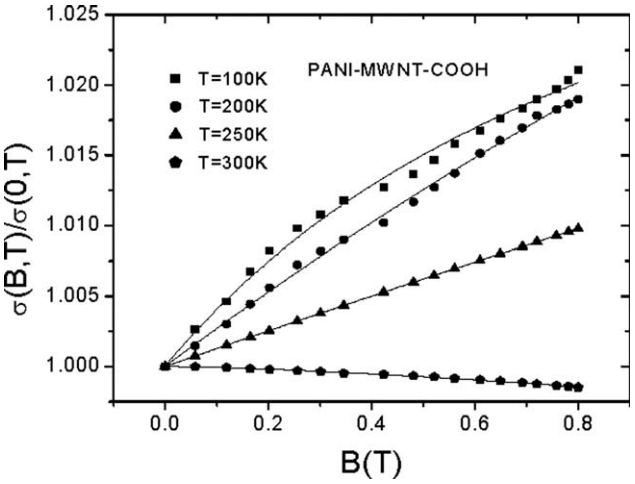

FIGURE 9 Variation of the dc magnetoconductivity with perpendicular magnetic field of PANI-MWNT-COOH sample at different temperatures. The solid lines are fitted to eq 5 for $T =$ 300 K and to eq 6 for $T =$ 250 K, 200 K, and 100 K.

Figure 9 shows the variation magnetoconductivity of PANI-MWNT-COOH sample for different temperature. The figure shows a change of sign in magnetoconductivity from negative to positive by decreasing the temperature. The positive magnetoconductivity provides a strong evidence to support that the average localization length of the composite is enhanced at low temperature. The magnitude of the magnetoconductivity decreases with increasing temperature and ultimately negative at a temperature $T = 300$ K due to the decrease of average hopping length. In Figure 9 the points are the experimental data while the solid lines represent the best fits obtained from eq 6 for temperature $T = 100$ K, 200 K, 250 K and from eq 5 for $T = 300$ K. It is evident from the Figure 9 that the experimental data can be well described by above theories. The localization length has been extracted from this fit and the average hopping length has also been calculated from the known values of L_{loc} and T_{Mott}. The average hopping length decreases from 60.5 to 12.6 nm with increasing temperature from 100 to 300 K, respectively which is consistent with the above analysis. Therefore, this anomalous behavior clearly indicates a transformation from quantum interference effect (low temperature) to the wave function shrinkage effect (room temperature) in PANI-MWNT-COOH sample.

CONCLUSIONS

PANI/CNT composites have been synthesized by an *in situ* chemical oxidative polymerization method with different MWNT and their structural, thermal stability, photoluminescence, and conductivity studies were carried out. The FTIR spectrum revealed that the product is PANI and shows the structural change by incorporation of CNT in PANI. Thermogravimetric analysis indicated a better stability for PANI with

different MWNT and CTAB has no affect on thermal stability of the composites. The maximum enhancement of photoluminescence intensity was observed in PANI-MWNT-COOH due to greater chances of exciton formation resulting from increased π electron mobility. It is observed from UV-Vis spectra that the optical bandgap increases by incorporating of different MWNT in PANI. The XRD results indicated that the carbon nanotubes existed in the composites and the peaks become much shaper for the composites due to the ordering of polymer chain along CNT. The SEM micrograph suggests that the aniline monomer is uniformly polymerized on the surface of the CNT and forms a columnal growth. We have measured the electrical conductivity of the investigated samples in the absence and also in the presence of the perpendicular magnetic fields. The room temperature conductivity σ (300 K) increases by introducing the highly conducting MWNT in polymer matrix. A linear variation of $\ln[\rho(T)]$ with $T^{-1/4}$ is observed in PANI, whereas in PANI/CNT composites two different slopes have been observed in $\ln[\rho(T)]$ versus with $T^{-1/4}$ plot. The values of T_{Mott} at higher temperature increase by one to two orders of magnitude when compared with the T_{Mott} at lower temperature. This suggests that the conductivity of the composites is dominated by CNT at lower temperatures. Because of the small average hopping length at room temperatures a negative magnetoconductivity was observed in PANI and PANI/CNT composites, which was interpreted by the wave function shrinkage effect. The average hopping length increases from 12.6 to 60.5 nm with decreasing temperature from 300 to 100 K, due to which the sign of the magnetoconductivity changes from negative to positive, which has been explained by the quantum interference effect.

The authors gratefully acknowledge the principal assistance received from the MHRD, Government of India during this work. A. K. Meikap thanks the TEQIP, Government of India for providing financial supports to come and live in Ireland.

REFERENCES AND NOTES

1 Naarman H. Science and Application of Conducting Polymers, Adam Hilger: Bristol, 1991.

2 Seanor, D. A. Electronic Properties of Polymer, Academic Press: New York, 1992.

3 MacDiarmid, A. G. Conjugated Polymers and Related Materials, Oxford University Press: London, 1993.

4 Reghu, M.; Cao, Y.; Moses, D.; Heeger, A. J. Phys Rev B 1993, 47, 1758–1764.

5 Skothemin, T. A.; Elsenbaumer, R. L. In Handbook of Conducting Polymers; Reynolds, J. R., Ed.; Marcel Dekker: New York, 1998.

6 Ghosh, M.; Barman, A.; Das, A.; Meikap, A. K.; De, S. K.; Chatterjee, S. J Appl Phys 1998, 83, 4230–4235.

7 Sarkar, A.; Ghosh, P.; Meikap, A. K.; Chattopadhyay, S. K.; Chatterjee, S. K.; Ghosh, M. J Appl Phys 2005, 97, 113713–113716.

8 Ghosh, P.; Sarkar, A.; Meikap, A. K.; Chattopadhyay, S. K.; Chatterjee, S. K.; Ghosh, M. J Phys D: Appl Phys 2006, 39, 3047.

9 Ajayan, P. M.; Stephan, O.; Colliex, C.; Trauth, D. Science 1994, 265, 1212–1214.

10 Thostensona, E. T.; Renb, Z.; Choua, T. W. Compos Sci Technol 2001, 61, 1899–1912.

11 Harris, P. J. F. Int Mater Rev 2004, 49, 31–43.

12 Baughman, R. H.; Zakhidov, A. A.; Heer, W. A. Science 2002, 297, 787–792.

13 Sandler, J.; Shaffer, M. S. P.; Prasse, T.; Bauhofer, W.; Schulte, K.; Windle, A. N. Polymer 1999, 40, 5967–5971.

14 Dalton, A. B.; Collins, S.; Munoz, E.; Razal, J. M.; Ebron, V. H.; Ferraries, J. P. Nature 2003, 423, 703.

15 Fan, S.; Chapline, M. G.; Franklin, N. R.; Tombler, T. W.; Cassell, A. M.; Dai, H. Science 1999, 283, 512–514.

16 Modi, A.; Koratkar, N.; Lass, E.; Wei, B.; Ajayan, P. M. Nature 2003, 424, 171–174.

17 Rao, C. N. R.; Satishkumar, B. C.; Govindaraj, A.; Nath, M. Chem Phys Chem 2001, 2, 78–105.

18 Curran, S. A.; Ajayan, P. M.; Blau, W. J.; Carroll, D. L.; Coleman, J. N.; Dalton, A. B.; Davey, A. P.; Drury, A.; Mccarthy, B.; Maier, S.; Strevens, A. Adv Mater 1998, 10, 1091–1093.

19 Cochet, M.; Maser, W. K.; Benito, A. M.; Callejas, M. A.; Martinez, M. T.; Benoit, J. M.; Schreiber, J.; Chauvet, O. Chem Commun 2001, 1450–1451.

20 Zengin, H.; Zhou, W.; Jin, J.; Czerw, R.; Smith, D. W., Jr.; Echegoyen, L.; Carroll, D. L.; Foulger, S. H.; Ballato, J. Adv Mater 2002, 14, 1480–1483.

21 Ago, H.; Petritsch, K.; Shaffer, M. S. P.; Windle, A. H.; Friend, R. H. Adv Mater 1999, 11, 1281–1285.

22 Kymakis, E.; Amaratunga, G. A. J Appl Phys Lett 2002, 80, 112–114.

23 Woo, H. S.; Czerw, R.; Webster, S.; Carroll, D. L. Synth Met 2001, 116, 369–372.

24 Wu, T. M.; Lin, Y. W.; Liao, C. S. Carbon 2005, 43, 734–740.

25 Yan, X.; Han, Z. J.; Yang, Yi.; Tay, B. K. J Phys Chem C 2007, 111, 4125–4131.

26 Jeevananda, T.; Siddaramaiah; Kin, N. H.; Heo, S. B.; Lee, J. H. Polym Adv Technol 2008, 19, 1754–1762.

27 Konyushenko, E. N.; Stejskal, J.; Trchova, M.; Hradil, J.; Kovarova, J.; Prokes, J.; Cieslar, M.; Hwang, J. Y.; Chen, K. H.; Sapurina, I. Polymer 2006, 47, 5715–5723.

28 Yu, Y.; Che, B.; Si, Z.; Li, L.; Chen, W.; Xue, G. Synth Met 2005, 150, 271–277.

29 Wei, Z.; Wan, M.; Lin, T.; Dai, L. Adv Mater 2003, 15, 136–139.

30 Sainz, R.; Benito, A. M.; Martinez, M. T.; Galindo, J. F.; Sotres, J.; Baro, A. M.; Corraze, B.; Chawet, O.; Maser, W. K. Adv Mater 2005, 17, 278–281.

31 Zhang, X.; Zhang, J.; Wang, R.; Liu, Z. Carbon 2004, 42, 1455–1461.

32 Zhang, X.; Zhang, J.; Liu, Z. Appl Phys 2005, A80, 1813–1817.

33 Long, Y.; Chen, Z.; Zhang, X.; Zhang, J; Liu, Z. Appl Phys Lett 2004, 85, 1796–1798.

34 Blanchet, G. B.; Fincher, C. R.; Gao, F. Appl Phys Lett 2003, 82, 1290–1292.

35 Feng, W.; Bai, X. D.; Lian, Y. Q.; Liang, J.; Wang, Z. G.; Yoshino, K. Carbon 2003, 41, 1551–1557.

36 Markavic, M. G.; Matisons, J. G.; Cervini, R.; Simon, G. P.; Fredericks, P. M. Chem Mater 2006, 18, 6258–6265.

37 Anglada, N. F.; Kaempgen, M.; Skakalova, V.; Weglikowska, U. D.; Roth, S. Diamond Relat Mater 2004, 13, 256–260.

38 Wu, M.; Snook, G. A.; Gupta, V.; Shaffer, M.; Fray, D. J.; Chen, G. Z. J Mater Chem 2005, 15, 2297–2303.

39 Germain, J.; Frechet, J. M. J.; Svec, F. J Mater Chem 2007, 17, 4989–4997.

40 Wu, T. M.; Lin, Y. W. Polymer 2006, 47, 3576–3582.

41 Zhang, X. Synth Met 2008, 158, 336–344.

42 Ali, S. R.; Ma, Y.; Parajuli, R. R.; Balogum, Y.; Lai, W. Y. C.; He, H. Anal Chem 2007, 79, 2583–2587.

43 Tasis, D.; Tagmatarchis, N.; Bianco, A.; Prato, M. Chem Rev 2006, 106, 1105–1136.

44 Kohlman, R. S.; Joo, J.; Epstein, A. J. In Physical Properties of Polymers Handbook; Mark, J., Ed; A. I. P.: New York, 1996.

45 Menon, R.; Yoon, C. O.; Moses, D.; Heeger, A. J.; Skotheim, T. A.; Elsenbaumer, R. L.; Reynolds, J. R. In Handbook of Conducting Polymers, 2nd ed.; Marcel Dekker: New York, 1996.

46 Philip, B.; Xie, J.; Abraham, J. K.; Varadam, V. K. Smart Mater Struct 2004, 13, N105–N108.

47 Wei, Z. X.; Wan, M. X.; Lin, T.; Dai, L. M. Adv Mater (Weinheim, Germany) 2003, 15, 136–139.

48 Quillard, S.; Louarn, G.; Lefrant, S.; MacDiarmid, A. G. Phys Rev B 1994, 50, 496–500.

49 Salaneck, W. R.; Lieberg, B.; Inganas, O.; Erlandsson, R.; Lundstrom, I.; MacDiarmid, A. G.; Halpern, M.; Somasiri, N. L. D. Mol Cryst Liq Cryst 1985, 121, 191–194.

50 Park, S. K.; Kim, S. H.; Hwang, J. T. J Appl Polym Sci 2008, 109, 388–396.

51 Amrithesh, M.; Aravind, S.; Jayalekshmi, S.; Jayasree, R. S. J Alloys Compd 2008, 449, 176–179.

52 Wise, D. L.; Wnek, G. E.; Trantlolo, D.; Cooper, T. M.; Gresser, J. D. Photonic Polymer Systems-Fundamentals, Methods and Applications; Marcel Dekker Inc.: New York, 1998.

53 Kane-Maguire, L. A. P.; MacDiarmid, A. G.; Norris, I. D.; Wallace, G. G.; Zheng, W. Synth Met 1999, 106, 171–176.

54 Mott, N. F.; Davis, E. Electronic Process in Noncrystalline Materials, 2nd ed.; Clarendon Press: Oxford, 1979.

55 Tauc, J. Amorphous and Liquid Semiconductors, Plenum Press: New York, 1974; pp 1–196.

56 Chaudhari, H. K.; Kelkar, D. S. Polym Int 1997, 42, 380–384.

57 Joo, J.; Long, S. M.; Pouget, J. P.; Oh, E. J.; MacDiarmid, A. G.; Epstein, A. J. Phys Rev B 1998, 57, 9567–9580.

58 Wang, Z. H.; Scherr, E. M.; MacDiarmid, A. G.; Epstein, A. J. Phys Rev B 1992, 45, 4190–4202.

59 Shklovskii, B. L. Sov Phys Semicond 1983, 17, 1311.

60 Shklovskii, B. L.; Efros, A. L. Electronic Properties of Doped Semiconductors; Springer: Berlin, 1994, p 202.

61 Nguyen, V. L.; Spivak, B. Z.; Shklovskii, B. I. Sov Phys JETP 1995, 62, 1021.

62 Sivan, U.; Entin-Wohiman, O.; Imry, Y. Phys Rev Lett 1988, 60, 1566–1569.

63 Rosenbaum, R.; Milner, A.; Hannens, S.; Murphy, T.; Palm, E.; Brandt, B. Physica B 2001, 294–295, 340–342.

64 Fuhrer, M. S.; Holmes, W.; Richards, P. L.; Delaney, P.; Louie, S. G.; Zettl, A. Synth Met 1999, 103, 2529–2532.

65 Yosida, Y.; Oguro, I. J Appl Phys 1999, 86, 999–1003.